

Photolysis of ClNO adsorbed on MgO(100)

L. HODGSON,¹ G. ZIEGLER,² H. FERKEL, H. REISLER, AND C. WITTIG

Department of Chemistry, University of Southern California, Los Angeles, CA 90089-0482

Received June 28, 1993

This paper is dedicated to Professor John C. Polanyi on the occasion of his 65th birthday

L. HODGSON, G. ZIEGLER, H. FERKEL, H. REISLER, and C. WITTIG. *Can. J. Chem.* **72**, 737 (1994).

The 365 nm pulsed laser photolysis of nitrosyl chloride adsorbed on a rough MgO(100) surface at 90 K has been studied. Mass spectrometric detection was used to record time-of-flight (TOF) spectra by monitoring Cl⁺ and NO⁺. These ions can derive from parent ClNO, which fragments completely in the mass spectrometer, as well as from Cl and NO photofragments. The TOF distributions are considerably slower than for the corresponding gas phase photodissociation process. NO was also detected state selectively by using resonance enhanced multiphoton ionization (REMPI), and a channel corresponding to direct adsorbate photolysis was identified. The state selective detection of NO molecules that emerge from the surface following photolysis shows unambiguously that their rotational degrees of freedom reflect the surface temperature ($T_{\text{rot}} = 100\text{--}140$ K), even at low coverages. At similar photolysis wavelengths, gas phase ClNO photodissociation is known to produce highly rotationally excited NO with a distinctive non-statistical distribution peaked at $J'' = 46.5$. Our studies suggest that, contrary to the gas-phase photolysis results, Cl and NO are not ejected rapidly following photolysis of surface-bound species on a repulsive potential energy surface. We postulate that ClNO grows in islands, with MgO defect sites serving as nucleation centers. Photofragment rotational and translational excitations are quenched efficiently due to strong attractive interactions that equilibrate NO to the surface temperature. Desorption of intact ClNO may also take place, but following (i.e., not during) the photolysis pulse. Such desorbed species can contribute to the TOF spectra, but not the REMPI spectra.

L. HODGSON, G. ZIEGLER, H. FERKEL, H. REISLER et C. WITTIG. *Can. J. Chem.* **72**, 737 (1994).

Opérant à 90 K, on a étudié la photolyse à 365 nm, par laser pulsé, du chlorure de nitrosyle adsorbé sur du MgO(100) rugueux. On a utilisé la détection par spectrométrie de masse en temps de vol (TOF) pour détecter le Cl⁺ et le NO⁺. Ces ions peuvent provenir du ClNO parent qui se fragmente complètement dans le spectre de masse ainsi que des photofragments Cl et NO. Les distributions dans les spectres en TOF sont beaucoup plus lentes que dans le cas du processus correspondant de photodissociation en phase gazeuse. On a aussi détecté sélectivement divers états du NO en faisant appel à la résonance par ionisation multiphotonique améliorée (REMPI) et on a identifié un canal correspondant à une photolyse directe de la substance adsorbée. La détection sélective d'états des molécules de NO qui émergent de la surface à la suite de la photolyse démontre sans ambiguïté que leurs degrés de liberté de rotation sont des reflets de la température à la surface ($T_{\text{rot}} = 100\text{--}140$ K), même à de faibles taux de couverture. À des longueurs d'onde de photolyse semblables, il est connu que la photodissociation en phase gazeuse de ClNO conduit à du NO dont l'excitation rotationnelle est élevée et qui présente une distribution non-statistique distinctive avec un sommet à $J'' = 46,5$. Nos études suggèrent que, contrairement aux résultats en photolyse en phase gazeuse, le Cl et le NO, sur une surface d'énergie potentielle répulsive, ne sont pas éjectés rapidement après la photolyse d'espèces liées à la surface. On fait le postulat que le ClNO croît sous forme d'îles sur les défauts des sites de MgO qui servent de centres de nucléation. Les excitations de rotation et de translation du photofragment sont désactivés efficacement à cause des fortes interactions qui permettent au NO de s'équilibrer avec la température de la surface. Il est possible que la désorption de ClNO intact puisse aussi se produire après (et non pas durant) la pulsation photolytique. De telles espèces peuvent contribuer au spectre de TOF, mais pas aux spectres REMPI.

[Traduit par la rédaction]

I. Introduction

The use of ultraviolet lasers to initiate photochemical transformations at gas-surface interfaces is an area of both technological importance and scientific interest. Potential applications involve areas of long-standing investment such as catalysis (1) and the photochemical deposition and etching processes that are used widely in the microelectronics industry (2). Topics of scientific interest include understanding the myriad photoinduced processes that occur on surfaces and the influence of the surface on the photodissociation dynamics of the adsorbate.

The photochemistry of adsorbates on metal surfaces is often quite complicated (3, 4). Direct adsorbate photodissociation has been seen on a few metal substrates (3), but this is frequently not the case. The substrate can quench photoexcited adsorbates, thereby minimizing direct adsorbate photolysis. Additionally, the substrate competes for absorption of the ultraviolet light needed for adsorbate photolysis. Substrate absorption can lead

to many different processes driven by photoemitted electrons, subvacuum level excitation, plasmon excitation, phonon excitation, etc. Reference 3 is an extensive review of the field of the photochemistry of adsorbates on metal surfaces.

Insulator surfaces typically transmit ultraviolet and visible light, making substrate-mediated processes less probable than on metal surfaces. This makes them better candidates for studying processes driven by adsorbate excitation. The direct photolysis of adsorbates on insulator surfaces has been seen in the following systems: CH₃Br (5–8), H₂S (6, 9), HBr (10, 11), HCl (11), OCS (12), C₂H₃Cl (13a), and NO₂ (13b) on LiF(001), CH₂I₂ on Al₂O₃ (14), Fe(CO)₅ on Al₂O₃ (15), thick polycrystalline layers of CH₃I on LiF(100) (16), C₆H₅I on LiF (17), CH₃I and CD₃I on MgO(100) (18) and NO₂ on Al₂O₃(1120) (19). In addition, the photodissociation of HBr (20) and CH₃Br (21) on LiF(001), IBr (22) and ICl (23) on MgO(001), and CH₃I on MgO(100) (18c) have been examined theoretically.

The detection of products in most of these systems has been achieved by using time-of-flight (TOF) mass spectroscopy, and information has been obtained regarding the different types of photochemical processes taking place and the geometries of the

¹U.S. Department of Education Predoctoral Fellow.

²Present address: Böhringer, Mannheim, Germany.

molecules on the surface. Several groups have used resonance enhanced multiphoton ionization (REMPI) to detect reaction products (16–19). This has enabled photodissociation products to be detected unambiguously and state-selectively and, in certain cases, has enabled comparisons to be made with vibrational state distributions obtained from the photolysis of gas phase molecules (16, 18).

An important characteristic of most of the insulator systems studied previously has been the presence of two channels observed in TOF mass spectroscopy: a slow one corresponding to desorption of the parent molecule and a fast one corresponding to direct photolysis of the adsorbate. Different mechanisms for parent desorption were proposed: excitation of color centers leading to shock waves which cause desorption (5, 6, 8, 9, 12, 13), thermal heating (7), substrate quenching of excited adsorbates followed by desorption (17), explosive desorption (14, 16), and laser annealing where molecules in unstable sites desorb (15).

Another important issue is the pattern of adsorbate growth on the insulator surface. In metals, the adsorbate often wets the surface, since the surface–adsorbate bonds are much stronger than the adsorbate–adsorbate bonds (24). This is not always the case with inert insulators. For example, based on their temperature programmed desorption (TPD) data, Tabares et al. concluded that CH_3Br forms 3-dimensional islands on their 30 K $\text{LiF}(001)$ surface (7). Harrison, et al. found that CH_3Br wets $\text{LiF}(001)$, but at temperatures ~ 117 K (8), i.e., just below the desorption temperature. Polanyi and co-workers reported island formation for OCS (12c) and HBr (10, 11, 25) adsorbed at 85 K on $\text{LiF}(001)$ and CH_3I on TiO_2 (26). In addition, they observed photoejection of HBr clusters (27) and photoreactions of HBr dimers (11).

CINO was chosen for several reasons. Its gas phase photochemistry has been studied in great detail and exhibits several distinctive features (23–31). Dissociation takes place on a steep repulsive surface (28), and thus might occur before energy can be transferred to the surface. The NO product can be detected sensitively with REMPI, thereby providing unambiguous identification of NO photoproducts. In addition, rotational and vibrational state distributions can provide valuable dynamical information that is lacking in TOF studies. CINO has a low bond dissociation energy ($13\,000\text{ cm}^{-1}$) (29) and absorbs light throughout the visible and ultraviolet — spectral regions that are easily accessed with tunable dye lasers. The 300 K absorption spectrum consists of several broad absorption bands (32), which have recently been assigned (30). Its NO product state distributions, photofragment yield spectra, recoil anisotropy, rotational alignment, NO Λ -doublet populations and the nature of the orbitals involved in electronic transitions have been determined both experimentally and theoretically (28–31).

At 355 nm, gas phase CINO is excited via a parallel transition, $S_3(2^1A') \leftarrow S_0(1^1A')$, yielding rotationally hot NO, i.e., $J''_{\text{peak}} = 46.5$ (29, 30). Almost all of the NO is in $v'' = 0$. Both NO spin–orbit states are nearly equally populated and there is a large propensity to form the Λ -doublet component that has its Π orbital perpendicular to the plane of NO rotation (29, 30). These signatures facilitate the determination of how the MgO crystal affects the photodissociation dynamics of adsorbed CINO.

In the present study, CINO adsorbed at 90 K on a rough $\text{MgO}(100)$ surface was photolyzed at 365 nm. Species emanating from the surface were detected using a quadrupole mass spectrometer (QMS), and state distributions of NO fragments

were determined by using two-photon, two-frequency laser ionization (REMPI). Single crystal $\text{MgO}(100)$ is transparent to the 365 nm photolysis radiation, therefore substrate absorption and electron-induced processes seen on metal surfaces should be minimized. CINO is weakly bound to the inert insulator surface, thus perturbation of its ground electronic potential energy surface should be slight. Due to this weak bond to the surface, island formation is likely. On the other hand, the nature of the electronically excited states of surface-bound CINO is presently unknown. Specifically, these may interact more strongly with the substrate than does ground state CINO. Therefore, we leave open the possibility that excited state dynamics of surface bound species differ qualitatively from those of their gas phase counterparts.

Following irradiation, TOF distributions are obtained by monitoring Cl^+ and NO^+ . Since parent CINO fragments completely in the mass spectrometer, yielding Cl^+ and NO^+ , the TOF spectra contain contributions from CINO molecules that desorb intact following irradiation, as well as from Cl and NO emerging from the surface. The TOF distributions are considerably slower than for the corresponding gas phase photodissociation process (28). This indicates a qualitative difference in the behavior of CINO following photoexcitation. Specifically, there is no evidence for rapid ejection of products from the surface. The NO rotational distributions obtained by using REMPI are cold and can be fit with $T_{\text{rot}} = 100\text{--}140$ K, which differs greatly from the highly non-statistical gas phase distributions. These results, together with temperature programmed desorption (TPD) data, suggest that CINO photolysis is dominated by strong attractive interactions with its surroundings and that CINO aggregates as islands on the surface, nucleating around defect sites.

The main focus of the present paper is twofold: (i) demonstrating unambiguously the remarkable difference between the photophysics and photochemistry of adsorbed versus gas phase CINO; and (ii) examining the possibility that nucleation and growth that takes place around defect sites are responsible for the observed differences.

II. Experimental

The experimental arrangement was described in detail elsewhere (33). Therefore only a brief description will be given, emphasizing modifications introduced for the photodissociation experiments. The vacuum system consisted of three chambers: a source chamber containing the molecular beam, a buffer chamber, and an ultrahigh vacuum (UHV) chamber. Figure 1 shows the UHV chamber, the major components being a rotatable sample manipulator equipped with liquid nitrogen cooling, two quadrupole mass spectrometers (UTI 100C), an Auger electron spectrometer (PHI 3017 with a 0.6% resolution CMA), a fast argon gun (Ion Tech), a channeltron electron multiplier (Galileo) for ion detection, a photolysis laser and a probe laser. The fast argon gun is not shown. The probe laser enters the chamber from below and ionizes NO 2–3 cm from the surface.

CINO (Matheson, 99.2%) was purified in several freeze–pump–thaw cycles with a pentane slush (-131°C). The sample was stored at liquid nitrogen temperature and used in a darkened glass bulb. The crystal was dosed with CINO using a pulsed molecular beam (Physik Instrumente). All experiments were performed at a backing pressure of 40–60 Torr neat CINO. This low backing pressure was necessary to attain low coverages of the crystal, and to avoid clustering of CINO in the molecular beam, which may become a problem with the greater cooling obtained at higher backing pressures. The coverage on the surface was varied by either changing the opening of the nozzle by controlling the voltage on the piezoelectric crystal, or by varying the dosing time, Δt . The product of Δt and the pressure increase in the

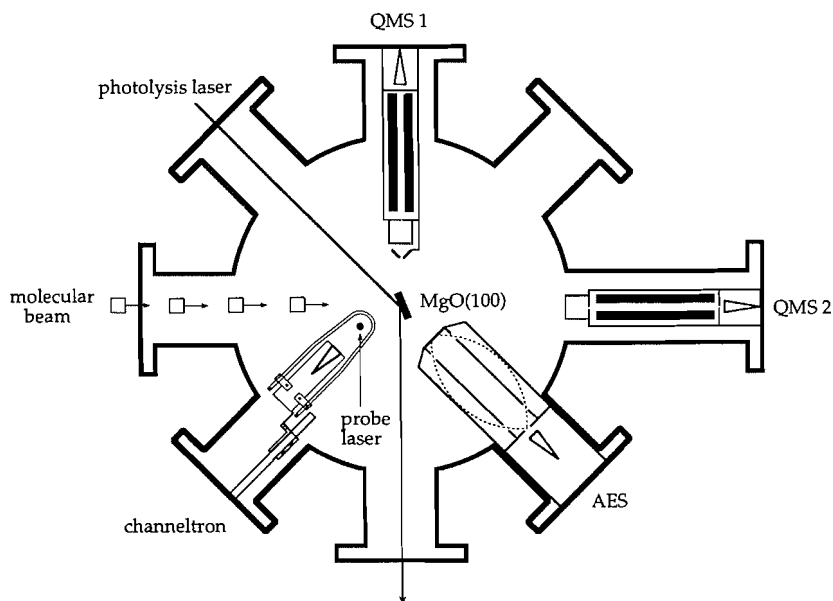


Fig. 1. Schematic of the UHV chamber for the adsorbate photolysis experiments. The photolysis radiation is incident on the MgO(100) crystal. The probe beam enters from below and ionizes NO 2–3 cm from the surface.

source chamber upon switching on the molecular beam, Δp , was proportional to coverage.

The MgO(100) crystal (Atomerigic, $10 \times 10 \times 1 \text{ mm}^3$) was cleaved and polished by the manufacturer. It was mounted on a molybdenum block which could be resistively heated to 800 K. Ideally, temperatures of $\sim 1100 \text{ K}$ would be needed for complete annealing. In our case, the surface can be characterized as clean but rough, exhibiting many steps, kinks, and vacancies. The surface temperature was measured using a chromel–alumel thermocouple attached to the molybdenum clamp of the sample holder. A temperature controller interfaced to a computer controlled the heating rate for the TPD experiments. The surface temperature was normally ramped at a rate of 0.5 K/s.

The surface was cooled with an open loop liquid nitrogen flow system. Liquid nitrogen flowed from a dewar outside the apparatus through an insulated feedthrough into the UHV chamber. Inside, flexible stainless steel bellows (connected to a small liquid nitrogen reservoir) and a sapphire plate joined the molybdenum surface holder to the reservoir. The sapphire acted as a thermal switch permitting cooling down to 90 K as well as high temperature annealing. Auger electron spectra (AES) of the MgO crystal could be taken at room temperature with a primary energy of 3 keV, but not always at liquid nitrogen temperature due to charging of the crystal. By reducing the primary energy to 800 eV, as suggested by Wei (34), reliable AES spectra could be obtained. Carbon was the main contaminant of the MgO crystal, as seen by the Auger spectrometer. This contamination was removed by fast argon atom bombardment (3 min, $\sim 0.01 \text{ mA}$ emission) followed by annealing (800 K, $\sim 1 \text{ h}$). Auger spectroscopy is not very useful for quantitatively determining coverage if the molecules are weakly physisorbed, since the high energy electrons may cause desorption as well as dissociation.

A quadrupole mass spectrometer oriented in line with the ClNO molecular beam (QMS 2 in Fig. 1), was used to determine the composition of the direct molecular beam. The ion signals from the direct beam consisted of Cl^+ and NO^+ in a ratio of 1:5. Parent ClNO completely fragmented in the ionizer. Another mass spectrometer, QMS 1, collimated with $\sim 5.5^\circ$ angular resolution, was used to detect products in the TPD and TOF experiments. The surface to ionizer distance was 8.4 cm.

The photolysis laser was a XeCl excimer (Questek 2200) pumped dye laser system (Lambda Physik, FL 2002) operating at 365 nm. In order to obtain a uniform beam profile, the beam was expanded using a telescope and only the center portion was used. The laser beam diameter could be varied from 1 to 5 mm. For TOF measurements the laser

beam diameter was 4–5 mm with energies of $\sim 250 \mu\text{J}$. The photolysis laser entered and exited the UHV chamber through quartz windows.

The rotational state distribution of NO molecules leaving the surface after photolysis was measured by REMPI. The probe laser was a Nd:YAG pumped tunable dye laser system (Quanta-Ray DCR2/PDL1) that was frequency doubled and Raman shifted. The 226 nm photons ($\sim 4 \mu\text{J}$) excite the NO $\gamma(0-0)$ transition and the 280 nm photons ($\sim 1 \text{ mJ}$) ionize the NO. The detection laser system was described in detail previously (33). The NO^+ ions were extracted from the ionization region and detected with a high sensitivity channeltron.

The determination of surface coverage on insulator surfaces by TPD is difficult. The difference in bond energies, i.e., between substrate–adsorbate and adsorbate–adsorbate is too small to produce a distinguishable break in the TPD spectra indicating the onset of multilayer coverage. The possibility of island growth further complicates the issue. In order to quantitatively determine the ClNO dosage in this experiment, a method commonly used for ionization gauge calibration was used. It makes use of the fact that the flux of molecules from a pressure stabilized reservoir through a known conductance into an evacuated chamber is fully computable (35). This flux calibration is reliable for molecules such as N_2 for which ionization gauge calibration factors are available. For a molecule such as ClNO, the flux must be calibrated through comparison with N_2 .

The determination of the sticking probability was achieved by dosing the surface with a ClNO molecular beam, and comparing the background pressure in the UHV chamber when the surface was maintained alternately well below and well above the ClNO desorption temperature. The sticking probability is close to zero for temperatures higher than the desorption temperature. The pressure component due to the molecular beam decreased when the temperature of the surface was lowered beneath the desorption temperature, indicating that ClNO sticks to MgO. If all molecules that hit the surface are adsorbed, the molecular beam component would be zero. A reduction of the molecular beam contribution of 50% was obtained, indicating a sticking probability of $\sim 50\%$ at a surface temperature of 90 K. There were no indications that heating the surface affected the pumping speed due to the change in cold areas cryopumping the chamber. This is a reasonable assumption due to the small area of the surface.

III. Experimental results

A. Temperature Programmed Desorption (TPD)

TPD was used to help determine the nature of ClNO adsorption. In Fig. 2, the Cl^+ and NO^+ mass spectrometer signals ver-

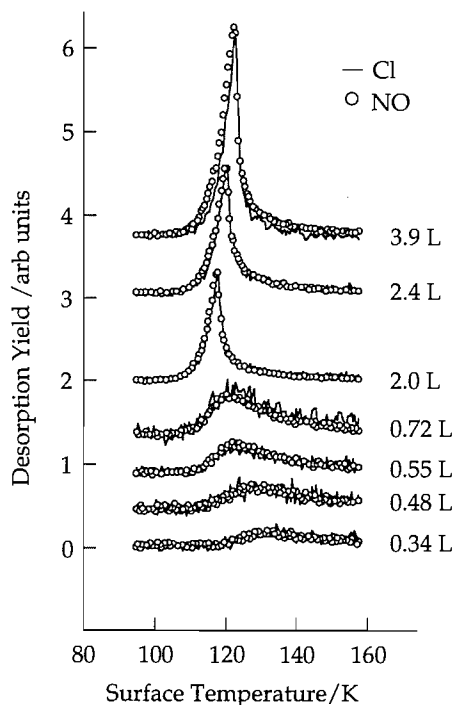


FIG. 2. TPD spectra of Cl^+ (lines) and NO^+ (circles) at different coverages with a heating rate of 0.5 K/s.

sus temperature, obtained at a heating rate of 0.5 K/s, are shown for different coverages. In each case, the Cl^+ and NO^+ signals were normalized to the same height, and the curves are offset for clarity. As mentioned previously, parent CINO cannot be seen due to complete fragmentation in the QMS. However, CINO most likely adsorbs molecularly on $\text{MgO}(100)$ since the desorption peaks for Cl^+ and NO^+ both occur at the same temperature. No other peaks were present in the TPD spectra, indicating that CINO does not dissociate or react to form other molecules on the surface. It also does not thermally decompose during TPD and the sample is not contaminated, though NO cannot be completely eliminated because of an equilibrium between CINO, NO, and Cl_2 (29). The main desorption peak for NO on $\text{MgO}(100)$ was below the lowest temperatures attainable (~ 90 K), so its presence is restricted to defect sites.

B. TOF following laser irradiation

Samples with CINO adsorbed on $\text{MgO}(100)$ were irradiated at 365 nm and species that subsequently leave the surface were detected with the QMS. Cl^+ and NO^+ were the only ions seen in the mass spectrometer and no positive ions were seen with the ionizer off. TOF data were typically taken with the photolysis laser wavevector at 45° to the surface normal. Products were detected with the surface facing QMS 1. Signals from the first 3–4 laser shots were discarded.

The data presented in Fig. 3 show TOF distributions for a coverage of 2.2 L. Signals were corrected for the velocity dependent QMS detection efficiency and the ion flight times in the QMS. The Cl^+ and NO^+ signals are normalized to the same height and their risetimes are almost identical. The NO^+ signal exhibits a tail due to background NO; when this is subtracted the signal is essentially the same as that of Cl^+ . Such data alone do not enable us to distinguish between CINO molecules that reach the mass spectrometer intact, as opposed to Cl and NO

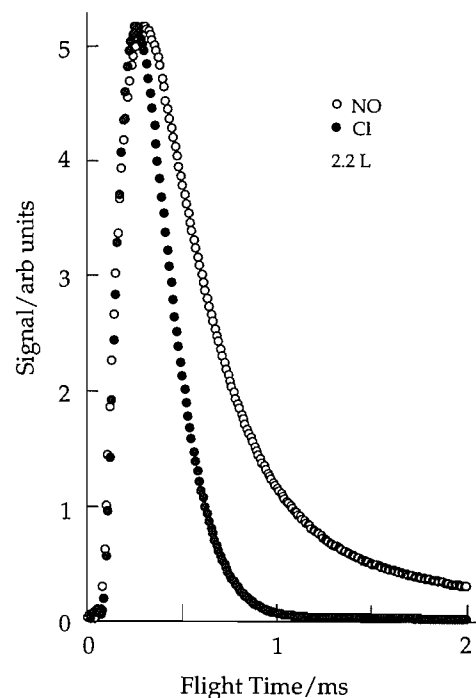


FIG. 3. Cl^+ (●) and NO^+ (○) TOF signals after 365 nm photolysis of 2.2 L of CINO adsorbed on $\text{MgO}(100)$. Velocity dependent ionization efficiencies and ion flight times in the QMS have been taken into account. The signals were normalized to the same peak intensity.

fragments that travel from the surface to the mass spectrometer. Thus, we conclude that the TOF signals may include contributions from both desorbed parent CINO and Cl and NO fragments generated in the photolysis of surface-bound CINO. Details will be given in a future publication.

C. Photodissociation cross section of adsorbed CINO

An upper limit to the CINO photodissociation cross section can be obtained from the variation of the NO^+ signal versus the number of laser pulses, for specific initial coverages. Time integrated NO^+ signals were obtained with the surface normal pointing towards QMS 1. Signals decrease with the number of pulses directed at the same spot on the surface due to adsorbate depletion. This variation depends on initial coverage, as shown in Fig. 4a. The laser intensity was kept constant throughout these measurements.

Several conclusions can be drawn from the plots presented in Fig. 4. NO^+ signals only decrease exponentially at low coverages and for a modest number of laser firings. At higher coverages, they are almost constant. This suggests that species from the topmost layers are being released into the gas phase upon irradiation. If the total photoexcitation cross section, σ , is independent of coverage, the signal at low coverages is given by (3)

$$[1] \quad S = S_0 \exp(-n\sigma\Phi)$$

where S is assumed to be proportional to the surface coverage; S_0 is the corresponding signal for the first laser shot; Φ is the number of photons per unit area; and n is the number of laser pulses. Because of the likelihood that some parent molecules are desorbed intact from the surface, the parameter σ should be interpreted as an upper limit to the photodissociation cross section. From the slope of the low coverage curve shown in Fig. 4b,

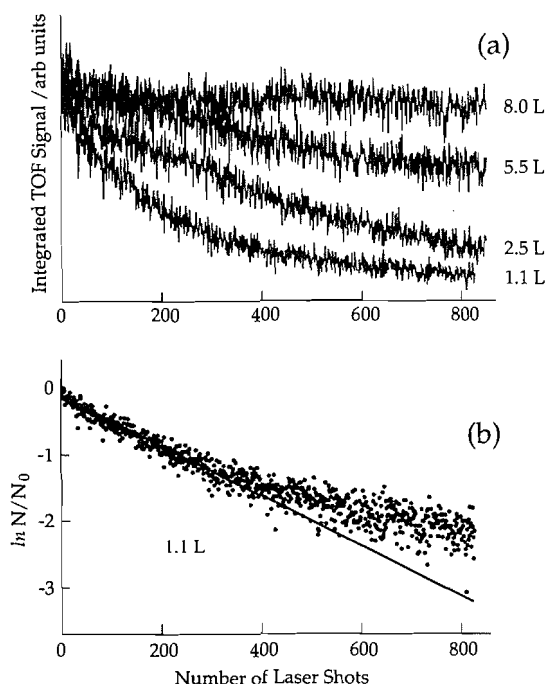


FIG. 4. Panel (a) shows the decrease in the time-integrated NO⁺ TOF signal when ClNO is photolyzed at 365 nm at various coverages. Panel (b) is a semilogarithmic plot of the signal versus photon fluence at low coverages, from which an upper bound to the photodissociation cross section is obtained.

σ can be determined. This curve is not purely exponential, as can be seen from the deviation from a straight line after ~ 400 laser shots. Such deviation at longer times was also seen with Fe(CO)₅ adsorbed on Al₂O₃ (15). This probably arises because the laser beam is not spatially homogeneous: if the beam is more intense at the center, the signal will be dominated by this region initially, but as molecules at the center are depleted, contributions from the lower intensity wings will begin to dominate. From the initial slope we derive $\sigma \sim 4 \times 10^{-19}$ cm². As stated above, this is an upper limit to the ClNO absorption cross section, since parent molecules that desorb following irradiation contribute to the observed signal decrease just as if they had been dissociated. This upper bound can be compared to the known gas phase absorption cross section of approximately 0.8×10^{-19} cm² (32). Additionally, interference between the incident, transmitted, and reflected radiation was not taken into account (12). No pronounced surface-enhanced photodissociation was seen, as has been reported for rough metal surfaces (36, 37) and for OCS on unannealed LiF(001) (12*a,b*). We also note that the QMS samples a small solid angle ($\sim 5.5^\circ$), while for accurate cross section measurements all particles must be detected, i.e., angular distributions may vary with coverage, as noted by Polanyi and co-workers (9).

D. State-specific NO detection by REMPI

NO($v''=0$) rotational distributions were determined by using REMPI. A scan over transitions in the region 225.7–227.0 nm required about 800 points, averaging 10 shots per point. Thus, stability of the experimental conditions over 8000 shots of the photolysis laser was necessary. At low coverages, when the signal drops exponentially with each laser pulse, this requirement could not be fulfilled without replenishing the surface. For

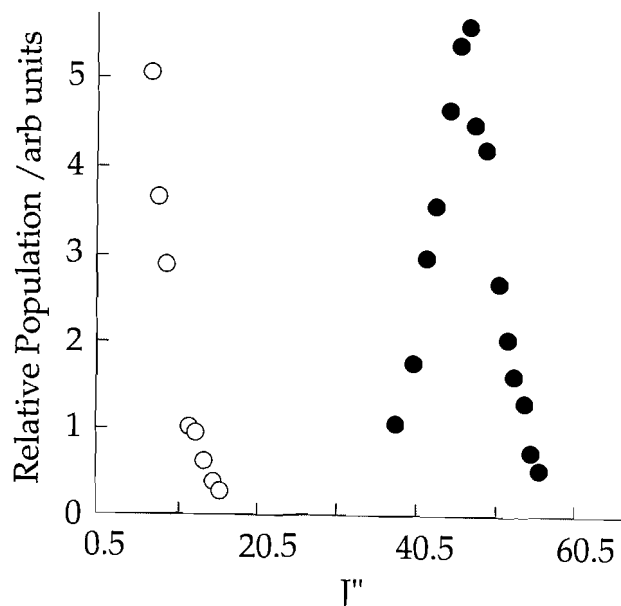


FIG. 5. Open circles: NO($v''=0$) rotational distribution from the 365 nm photolysis of ClNO adsorbed on MgO(100). Data are for the R₁₁ + Q₂₁ branch of the lower energy ²Π_{1/2} spin-orbit state; they can be fit with $T_{\text{rot}} \sim 140$ K. Filled circles: NO($v''=0$) rotational distribution from 355 nm photolysis of gas phase ClNO. Data are for the Q₁₁ + P₂₁ branch of ²Π_{1/2}.

example, an initial coverage of about 1 L would be removed with 3000 laser shots.

By using the pulsed molecular beam as a doser, the crystal could be dosed between photolysis laser pulses, thereby maintaining a steady state of molecules on the surface during the measurement (5–13, 16, 38). The molecular beam and photolysis laser both operated at 10 Hz. Typical steady state surface coverages were 0.2–0.8 L. The stable signals obtained by using this alternating dose-and-desorb condition have proven to be invaluable for measurements of NO rotational distributions. With the surface positioned as shown in Fig. 1, rotationally resolved spectra were obtained under steady state conditions. Results are summarized as the open circles in Fig. 5 for a coverage of ~ 0.5 L. The time delay between the photolysis and probe laser was optimal at 150 μ s. The data shown are for the R₁₁ + Q₂₁ branch in the lower energy ²Π_{1/2} spin orbit state. The NO rotational distributions corresponded to $T_{\text{rot}} = 100$ –140 K — remarkably different from the hot NO rotational distributions seen in gas phase photolysis (29, 30) and reproduced in Fig. 5 (filled circles). No NO($v''=1$) was detected, paralleling the gas phase photolysis results, in which very little NO($v''=1$) is produced.

IV. Discussion

A. Evidence for adsorbate photodissociation

The results presented above indicate that the TOF and REMPI signals are a consequence of irradiating samples in which ClNO is adsorbed molecularly on MgO(100). We checked for contributions from gas phase ClNO photodissociation by the 365 nm photolysis laser, since the background pressure in the UHV chamber increased slightly when the molecular beam was on. With the molecular beam on and the crystal at 300 K (i.e., too high a temperature for ClNO to

adsorb), no signal was seen with the QMS, confirming that the observed signals are associated with molecules that are adsorbed on the crystal. The most convincing evidence against gas phase photodissociation, however, comes from the NO rotational distributions, which differed remarkably from those obtained in the gas phase photolysis of ClNO at any wavelength.

All signals depend linearly on 365 nm fluence over a large range of coverages, and therefore are not due to photodesorption of ClNO followed by its photolysis. Note that this rules out photodissociation of gaseous ClNO that is desorbed *within* the laser pulse, but leaves open the issue of ClNO that desorbs *following* the photoexcitation pulse. Signals were also checked for photodissociation of ClNO by the probe laser, since the absorption cross section of ClNO at 226 nm is a factor of 10^2 higher than at 365 nm (32). The laser signal depended on one photon each of the 226 and 280 nm radiations, confirming that absorption of the probe laser light by background ClNO is insignificant. This is also expected on the basis of the 226 nm photon fluence and the ClNO absorption cross section: only $\sim 10^{-4}$ of the ClNO will be photodissociated. The most conclusive evidence for direct photodissociation of adsorbed ClNO comes from the observation of NO by REMPI under conditions where photodissociation of desorbed ClNO is insignificant.

Preliminary experiments at other photolysis wavelengths are consistent with the suggestion that adsorbate photodissociation is taking place. Though fragments were detected following 475 nm photolysis (which coincides with the ClNO $S_1 \leftarrow S_0$ system), almost no signal was seen following irradiation in the weak $T_1 \leftarrow S_0$ system near 600 nm. At 600 nm, the cross section for gas phase ClNO photodissociation is small compared to 475 and 365 nm (32). It is also possible that surface and bulk defects, as well as photoproducts that remain bound to the surface (e.g., at defects), have absorptions that vary throughout these wavelength ranges.

B. Island formation

MgO(100) has many surface defects (predominantly oxygen vacancies) (39). Electrons can be trapped at these sites, creating states within the 7.8 eV band gap (40). States located 2.3 and 6 eV below the vacuum level have been seen by Henrich et al. using electron energy loss spectroscopy and were discussed in terms of oxygen vacancies and intrinsic surface effects (39). One indication of the existence of such defect states on the rough MgO(100) crystal used in the present experiments is the observation of a blue fluorescence upon electron bombardment. This fluorescence could be seen readily by the eye and was strongest for a clean MgO surface. After exposure to ClNO and desorption of ClNO by heating the surface ~ 150 K, the fluorescence disappeared and a small amount of chlorine could be seen on the surface with AES. This suggests that some ClNO dissociatively adsorbs on the surface with the chlorine occupying defect sites in the MgO crystal, most likely oxygen vacancies. These Cl atoms are strongly bound. They cannot be removed at temperatures as high as 800 K, but they can be removed with fast argon bombardment. Thus, it is possible that the nucleation center is a Cl atom attached to a defect.

The temperature at which exposures were carried out prior to TPD is only ~ 30 K lower than the main desorption peak at ~ 120 K. We assume that, following ClNO adsorption at 90 K, molecules are able to diffuse across the surface and may either find an unoccupied defect site, or may collide with other

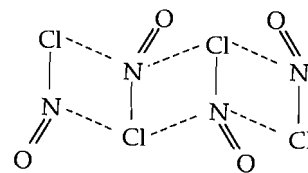


FIG. 6. Molecular solid of ONCl-II as proposed by Jones and Swanson (44).

so-called "walkers" (41), as well as with islands already formed. At higher exposures, defect-free areas become covered, presumably beginning with sites adjacent to the decorated defects. In this picture, adlayer growth over defect-free areas is in the form of two-dimensional islands and is nucleated by decorated defects. It should be mentioned that an island randomly formed on a defect-free area is not necessarily stable and can decay before exceeding the critical size to become stable (42). Therefore, the density on the surface during dosing can influence the ultimate size distribution of islands, at least at low coverage. Dosing the surface with a pulsed molecular source may cover the surface somewhat differently than a doser that maintains a constant density on the crystal after initiating the dosing procedure.

Desorption between 120 and 140 K is attributed to molecules evaporating from defect-free areas, perhaps at the edge of islands or dendrites. The desorption peak is seen to shift to lower temperatures with increasing coverage (Fig. 3). In general, such behavior of a TPD peak can be indicative of a variety of phenomena, including recombinative desorption (following dissociative adsorption), collision mediated desorption, and repulsive lateral interaction. Simulations of the TPD results indicate that the magnitude of the observed shift is consistent with each of these. At higher coverages, zeroth order desorption (typical of multilayers, clusters and chains of molecules) is seen.

Some information regarding ClNO aggregates can be obtained from spectroscopic studies of ClNO ices and thin films. Killough et al. (43) showed that in the range 85–190 K, ClNO ice exists as covalent dimers (ONCl-II), while in the range 74–85 K, an ionic phase exists (ONCl-I). Later, Jones and Swanson used infrared spectroscopy to study ClNO in matrices and thin films deposited on a cold CsI window (44). They suggested that ONCl-II consists of long chains with strong intermolecular covalent bonds, as shown in Fig. 6. This geometry agrees with *ab initio* calculations which show that nitrogen has a partial positive charge while chlorine and oxygen have partial negative charges (30). Formation of these chains leads to weakening of the Cl—NO bonds. The surface temperature of ~ 90 K used in our study is near the ONCl-I/ONCl-II phase transition. Dimer or chain formation is consistent with our observation of islands. However, if ClNO is ionic when adsorbed on the ionic MgO crystal, comparison to the gas phase photochemistry may be unjustified. A direct determination of the geometry and structure of ClNO on MgO(100) is clearly needed.

C. Rotational and translational energy distributions

As stated earlier, NO rotational distributions were very cold (100–140 K), i.e. close to the surface temperature. This differs markedly from the rotationally hot distributions seen in gas phase photodissociation.

As stated above, the TOF distributions observed mass spec-

trometrically may originate both from desorbed ClNO and photodissociation fragments. However, the observed distributions all correspond to species that are traveling much more slowly than in the case of gas phase photodissociation and there is no indication of a fast, instantaneous component. We note that the desorbates have average kinetic energies of ~ 10 meV, while in the gas phase photodissociation of ClNO, the Cl and NO fragments have 580 and 670 meV of translational energy, respectively, in the center-of-mass system. These values were obtained by assuming that 70% of the available energy goes into translation, as reported for the gas phase photolysis of ClNO at 347 nm by Busch and Wilson (28).

The observed cold translational and NO rotational energy distributions at nominal submonolayer coverages are consistent with island formation, where photofragments can experience strong, attractive interactions with other molecules in the island and the surface before escaping. Thus, their translational and rotational energies are quenched and are quite different from the products of gas phase photolysis. Similar TOF spectra were also seen with CH₃I on LiF (16) and HBr islands on LiF(001) (11) and interpreted in terms of products formed in lower layers which undergo many collisions before escaping. In the case of HBr, the H-atom TOF low energy tail increased with surface coverage.

It is surprising that other products (e.g., Cl₂) were not detected. In many systems, species other than the parent and photolysis products have been seen, indicating photoinitiated reaction (PRXN) on the surface (6, 9–11, 12c, 13, 17, 18). In these cases, surface-bound molecules are aligned due to interactions with the surface as well as each other and photolysis initiates reaction with an adjacent molecule. Attack angles and impact parameters are restricted, leading to a surface aligned PRXN.

It is known that the gas phase reaction $\text{Cl} + \text{ClNO} \rightarrow \text{Cl}_2 + \text{NO}$ has a large rate constant (45), and produces vibrationally excited NO (46). Thus, Cl₂ is potentially a PRXN product. However, no signal was observed at $m/e \cong 71$, indicating that the Cl⁺ signals do not derive from Cl₂. Moreover, Cl₂ does not stay on the surface, since TPD spectra (to 200°C) taken after as many as 100 laser shots were identical to those taken with the photolysis laser off. The binding energy of Cl₂ to MgO has recently been calculated to be 4.1 kcal/mol (47). Thus, the photolysis laser does not initiate the formation of other products on the surface. The absence of a PRXN may result from the restricted geometries of surface-bound molecules. More work is needed to clarify this point.

Although the exact geometry of ClNO on the surface is unknown, it is reasonable that it lies flat on the surface, in analogy with the suggested geometry of its thin films on CsI surfaces (Fig. 6) (44). Consequently, photoproducts may be ejected preferentially in the plane of the surface. Since TOF products were typically detected along the surface normal, our observations may be biased toward molecules that undergo collisions. To examine this, TOF distributions were obtained with the detector at the surface normal and at 45° to the normal. Both measurements gave identical results. Though this is consistent with there being no surface order, it is also consistent with the surface being too rough for its plane to be well defined.

The TOF distributions obtained by Polanyi and co-workers for CH₃Br adsorbed on rough LiF also indicated slow products relative to smooth surfaces or gas phase photodissociation (6, 8). They attributed this to strong adsorption at different defect

sites. The reduced translational energy was attributed to increased internal energy of the fragments and/or energy transfer to the surface, since bonding to the defect is strong. In our case, NO has *less* internal energy than in the corresponding case of gas phase photodissociation. After photodissociation the fragments may stick to the surface before desorbing. For example, Watson, NoorBatcha, and Lucchese (21), in trajectory simulations of the 222 and 193 nm photodissociation of CH₃Br on LiF(001), see a significant amount of sticking, especially on a rough surface. With our time resolution, it is not possible to determine if molecules stick briefly before desorbing.

Obviously the situation is complex and without knowing the geometry and nature of the surface-bound molecules it is imprudent to propose a complete model. It is unknown whether ClNO on the surface adsorbs in planar or non-planar geometries, and whether its structure is covalent, ionic, a molecular chain, or a 2- or 3-dimensional island. Presently experiments are being conducted to determine the nature of the bonding and the geometry of the molecules on the surface. In addition, experiments on smooth MgO crystals aimed at further establishing the role of defect sites are in progress in our laboratory (48). Preliminary results from these latter experiments confirm the interpretation suggested in this paper.

V. Conclusions

This study establishes that ClNO adsorbs molecularly on rough MgO(100) surfaces at 90 K. Following 365 nm laser irradiation, products due to ClNO photolysis are unambiguously identified by REMPI. TOF distributions indicate that only very slow species emanate from the surface. The NO⁺ and Cl⁺ mass spectrometer signals are probably due to both photodissociation and cracking of desorbed parent ClNO. The slow TOF distributions are remarkably different than gas phase photolysis, which yields high translational energies of products. NO rotational distributions reflect the surface temperature ($T_{\text{rot}} = 100\text{--}140$ K) and, again, are much colder than the corresponding gas phase distributions which peak at $J'' = 46.5$, suggesting that strong attractive interactions with the surface take place prior to desorption. Evidence points to ClNO island formation, with nucleation occurring around defect sites, but the nature and geometry of ClNO on the surface are presently unknown. One possibility is the chain-like structure observed by Killough et al. on cold CsI. Work is currently in progress to determine the geometry of ClNO on MgO(100), and the role of defects on the dissociation.

Acknowledgments

The authors thank Bruce Koel, Scott Powers, and Peter Blass for many helpful discussions and Jessie Chu and James Singleton for technical assistance. This research was supported by AFOSR.

1. T.J. Chuang, Surf. Sci. Rep. **3**, 1 (1983).
2. R.M. Osgood, Jr. Ann. Rev. Phys. Chem. **34**, 77 (1983).
3. X.-L. Zhou, X.-Y. Zhu, and J.M. White. Surf. Sci. Rep. **13**, 73 (1991).
4. X.-L. Zhou, X.-Y. Zhu, and J.M. White. Acc. Chem. Res. **23**, 327 (1990).
5. E.B.D. Bourdon, J.P. Cowin, I. Harrison, J.C. Polanyi, J. Segner, C.D. Stanners, and P.A. Young. J. Phys. Chem. **88**, 6100 (1984).
6. E.B.D. Bourdon, P. Das, I. Harrison, J.C. Polanyi, J. Segner, C.D. Stanners, R.J. Williams, and P.A. Young. Faraday Discuss. Chem. Soc. **82**, 343 (1986).
7. F.L. Tabares, E.P. Marsh, G.A. Bach, and J.P. Cowin. J. Chem. Phys. **86**, 738 (1987).

8. I. Harrison, J.C. Polanyi, and P.A. Young. *J. Chem. Phys.* **89**, 1475 (1988).
9. I. Harrison, J.C. Polanyi, and P.A. Young. *J. Chem. Phys.* **89**, 1498 (1988).
10. E.B.D. Bourdon, C.-C. Cho, P. Das, J.C. Polanyi, C.D. Stanners, and G.-Q. Xu. *J. Chem. Phys.* **95**, 1361 (1991).
11. C.-C. Cho, J.C. Polanyi, and C.D. Stanners. *J. Chem. Phys.* **90**, 598 (1989).
12. (a) St. J. Dixon-Warren, I. Harrison, K. Leggett, M.S. Matyjaszczyk, J.C. Polanyi, and P.A. Young. *J. Chem. Phys.* **88**, 4092 (1988); (b) K. Leggett, J.C. Polanyi, and P.A. Young. *J. Chem. Phys.* **93**, 3645 (1990); (c) St. J. Dixon-Warren, K. Leggett, M.S. Matyjaszczyk, J.C. Polanyi, and P.A. Young. *J. Chem. Phys.* **93**, 3659 (1990); (d) J.C. Polanyi and P.A. Young. *J. Chem. Phys.* **93**, 3673 (1990).
13. (a) St. J. Dixon-Warren, M.S. Matyjaszczyk, J.C. Polanyi, H. Rieley, and J.G. Shapter. *J. Phys. Chem.* **95**, 1333 (1991); (b) St. J. Dixon-Warren, R.C. Jackson, J.C. Polanyi, H. Rieley, J.G. Shapter, and H. Weiss. *J. Phys. Chem.* **96**, 10983 (1992).
14. (a) T.J. Chuang and K. Domen. *J. Vac. Sci. Technol.* **A5**, 473 (1987); (b) K. Domen and T.J. Chuang. *J. Chem. Phys.* **90**, 3318 (1989); (c) T.J. Chuang and K. Domen. *J. Vac. Sci. Technol.* **B7**, 1200 (1989); (d) K. Domen and T.J. Chuang. *Phys. Rev. Lett.* **59**, 1484 (1987).
15. F.G. Celii, P.M. Whitmore, and K.C. Janda. *J. Phys. Chem.* **92**, 1604 (1988).
16. (a) J. Kutzner, G. Lindeke, K.H. Welge, and D. Feldmann. *J. Chem. Phys.* **90**, 548 (1989); (b) D. Feldmann, J. Kutzner, and K.H. Welge. *In Springer Ser. Surf. Sci. Vol. 19. Edited by G. Betz and P. Varga.* Springer-Verlag, Berlin. 1990.
17. E. Villa, J.A. Dagata, and M.C. Lin. *J. Chem. Phys.* **92**, 1407 (1990).
18. (a) K.A. Trentelman, H. Fairbrother, P.C. Stair, P.G. Strupp, and E. Weitz. *J. Vac. Sci. Technol.* **A9**, 1820 (1991); (b) K.A. Trentelman, D.H. Fairbrother, P.G. Strupp, P.C. Stair, and E. Weitz. *J. Chem. Phys.* **96**, 9221 (1992); (c) M.I. McCarthy, R.B. Gerber, K.A. Trentelman, P. Strupp, D.H. Fairbrother, P.C. Stair, and E. Weitz. *J. Chem. Phys.* **97**, 5168 (1992).
19. (a) T.J. Chuang, R. Schwarzwald, and A. Mödl. *J. Vac. Sci. Technol.* **A9**, 1719 (1991); (b) T.J. Chuang. *Lect. Notes Phys.* **389**, 203 (1991).
20. Z.-H. Huang and H. Guo. *J. Chem. Phys.* **96**, 8564 (1992).
21. (a) J.M. Watson, I. NoorBatcha, and R.R. Lucchese. *J. Chem. Phys.* **96**, 7771 (1992); (b) Z.-H. Huang and H. Guo. *J. Chem. Phys.* **97**, 2110 (1992); (c) Z.-H. Huang and H. Guo. *J. Chem. Phys.* **98**, 3395 (1993).
22. M.I. McCarthy, R.B. Gerber, and M. Shapiro. *J. Chem. Phys.* **92**, 7708 (1990).
23. M.I. McCarthy and R.B. Gerber. *J. Chem. Phys.* **93**, 887 (1990).
24. M. Wortis. *Phys. Today*, **38**, S-22 (1985).
25. J.C. Polanyi, R.J. Williams, and S.F. O'Shea. *J. Chem. Phys.* **94**, 978 (1991).
26. V.P. Holbert. Ph.D. Thesis, Northwestern University. 1991.
27. C.-C. Cho, J.C. Polanyi, and C.D. Stanners. *J. Phys. Chem.* **92**, 6859 (1988).
28. G.E. Busch and K.R. Wilson. *J. Chem. Phys.* **56**, 3655 (1971).
29. A. Ogai, C.X.W. Qian, L. Iwata, and H. Reisler. *Chem. Phys. Lett.* **146**, 367 (1988).
30. Y.Y. Bai, A. Ogai, C.X.W. Qian, L. Iwata, G.A. Segal, and H. Reisler. *J. Chem. Phys.* **90**, 3903 (1989).
31. C.X.W. Qian, A. Ogai, L. Iwata, and H. Reisler. *J. Chem. Phys.* **92**, 4296 (1990).
32. C.F. Goodeve and S. Katz. *Proc. R. Soc. London*, **A172**, 432 (1939).
33. E. Kolodney, P.S. Powers, L. Hodgson, H. Reisler, and C. Wittig. *J. Chem. Phys.* **94**, 2330 (1991).
34. W. Wei. *J. Vac. Sci. Technol.* **A6**, 2576 (1988).
35. Leybold Vacuum Products, Inc. Product and vacuum technology reference book.
36. A. Nitzan and L.E. Brus. *J. Chem. Phys.* **75**, 2205 (1981).
37. (a) G.M. Goncher and C.B. Harris. *J. Chem. Phys.* **77**, 3767 (1982); (b) G.M. Goncher, C.A. Parsons, and C.B. Harris. *J. Phys. Chem.* **88**, 4200 (1984).
38. E. Hasselbrink, S. Jakubith, S. Nettesheim, M. Wolf, A. Cassuto, and G. Ertl. *J. Chem. Phys.* **92**, 3154 (1990).
39. V.E. Henrich and R.L. Kurtz. *J. Vac. Sci. Technol.* **18**, 416 (1981).
40. V.E. Henrich. *In Advances in ceramics*, Vol. 10. Edited by W.D. Kingery. Am. Chem. Soc. Columbus, OH. 1984.
41. M.C. Bartelt and J.W. Evans. *Phys. Rev. B: Solid State*, **46**, 12675 (1992).
42. J.A. Venables, G.D.T. Spiller, and M. Hanbrücken. *Rep. Prog. Phys.* **47**, 399 (1984).
43. P.M. Killough, B.I. Swanson, and S.F. Agnew. *J. Phys. Chem.* **93**, 7953 (1989).
44. L.H. Jones and B.I. Swanson. *J. Phys. Chem.* **95**, 86 (1991).
45. J.P.D. Abbatt, D.W. Toohey, F.F. Fenter, P.S. Stevens, W.H. Brune, and J.G. Anderson. *J. Phys. Chem.* **93**, 1022 (1989).
46. A.J. Grimley and P.L. Houston. *J. Chem. Phys.* **72**, 1471 (1980).
47. M.I. McCarthy and A.C. Hess. *J. Chem. Phys.* **96**, 6010 (1992).
48. H. Ferkel, L. Hodgson, J. Singleton, P.M. Blass, H. Reisler, and C. Wittig. To be published.